Supplementary information

Stellar mergers as the origin of the blue main-sequence band in young star clusters

In the format provided by the authors and unedited

Supplementary Information: Stellar mergers as the origin of the blue main-sequence band in young star clusters

Chen Wang, Norbert Langer, Abel Schootemeijer, Antonino Milone,
Ben Hastings, Xiao-Tian Xu, Julia Bodensteiner, Hugues Sana, Norberto Castro,
D. J. Lennon, Pablo Marchant, A. de Koter, Selma E. de Mink

A: Procedure to identify blue main-sequence stars

The main characteristic feature in the distribution of the cluster stars in the CMD, which is the basis for our work, is that the MS band is split into two distinct components. This is a striking feature not only visible in the CMD of MS stars in NGC 1755, but rather a common feature detected in Magellanic Cloud star clusters younger than ~ 600 Myr [1]. In this work, we fix our attention on clusters younger than 100 Myr, whose distinct components can be compared with our models of stars exceeding 2 $M_\odot$. Currently, high-quality data exists for six clusters younger than 100 Myr in the LMC and the SMC (NGC 330, NGC 1818, NGC 1805, NGC 1755, NGC 1850 and NGC 2164), five of which are shown to exhibit the split MS (excluding NGC 1805), but one of them (NGC 1850) is composed of two sub-clusters [1]. We investigate all the remaining four clusters in this work, which are the LMC clusters NGC 1755, NGC 1818, NGC 2164 and the SMC cluster NGC 330. We use the observational data published in [1] which includes corrections for differential reddening. We use the same method as in that work to eliminate the contamination from the foreground and background field stars.

1

In this section, we illustrate the procedure to distinguish the blue and the red MS stars in young star clusters. We use a model-independent method similar to [2], that star classification is based on their split distribution in the CMD. We calculate the color difference between each observed star and a fiducial line that best describes the well-populated red MS in the CMD. To determine this fiducial line, we first draw a line along the red MS by visual inspection. Then we smooth this line by selecting a sample of red MS stars whose color distances to this line are smaller than four times the photometric error at corresponding magnitudes. We divide the selected red MS stars into bins of 0.2 mag. The final fiducial line is then determined by the median color and magnitude of the selected red MS stars in each magnitude bin (see the red line in Supplementary Figure 1a for NGC 1755). We draw the fiducial line from a magnitude below the cluster turn-off magnitude because the red and the blue MS stars are not well discernible near the turn-off.

Taking NGC 1755 as an example, in our considered area (Supplementary Figure 1b), we calculate the color difference $\Delta(m_{F336W} - m_{F814W})$ between each star and the fiducial line (Supplementary Figure 1c). Supplementary Figure 1d shows the histogram of $\Delta(m_{F336W} - m_{F814W})$ distribution in eight magnitude bins, with a bin size of 0.5 mag. We only display the results for stars with $\Delta(m_{F336W} - m_{F814W}) \leq 0.5$. Finally, we perform a bi-Gaussian fitting for $\Delta(m_{F336W} - m_{F814W})$ distribution. We remind the reader that this bi-Gaussian fitting depends somehow on which histograms are taken into account. To exclude the effect from potential binaries, in our bi-Gaussian fitting, we only include the histograms with $\Delta(m_{F336W} - m_{F814W})$ smaller than a critical value, which is 0.12 if $m_{F814W} \geq 20$, 0.1 if $19.5 \leq m_{F814W} < 20$, 0.08 if $19 \leq m_{F814W} < 19.5$, and 0.06 if $17 \leq m_{F814W} < 19$, taking into account the fact that $\Delta(m_{F336W} - m_{F814W})$ of a binary system with a specific mass ratio increases with magnitude. The dark grey and light grey histograms in Supplementary Figure 1d represent the histograms included and excluded in the bi-Gaussian fitting, respectively. As to the normalization, we first normalize the dark grey histograms to

an area of unity, which facilitates the bi-Gaussian fitting. Then we normalize the light grey histograms such that the ratio between the area of the light grey histograms and the dark grey histograms equals the number ratio of the stars excluded and included in the bi-Gaussian fitting.

We classify all stars with $\Delta(m_{F336W} - m_{F814W})$ smaller than the value at which the two Gaussian curves cross as blue MS stars. While at $m_{F814W} \leq 17$, we use eye inspection to identify blue MS stars according to isochrone fitting (Supplementary Information B). The final identified blue MS stars in NGC 1755 are indicated by the blue circles in Fig. 1b. The same procedure is used to identify the blue MS stars in NGC 330 (Supplementary Figure 2), NGC 1818 (Supplementary Figure 3) and NGC 2164 (Supplementary Figure 4). In NGC 330, we adopt a smaller $\Delta(m_{F336W} - m_{F814W})$ boundary in our bi-Gaussian fitting for the bright stars, which is 0.04 if $17.5 \leq m_{F814W} < 18$ and 0.02 if $17 \leq m_{F814W} < 17.5$.

B: The main sequence split as a function of stellar rotation

Rotation is widely accepted to be responsible for the split MS [3, 4, 5]. In this section, we explore how much rotation is required to retrieve the color split by comparing our rotating single star models with the MS components in the above mentioned four clusters. We next describe the physics and assumptions adopted while computing the single star models.

In the framework of a single star-burst forming a star cluster, (i.e., all stars are born at the same time), we attempt to use the isochrones constructed from our stellar models to fit the observations. The observations show a narrow red MS band, which marks the peak of stellar density in the CMD. In particular below 19th magnitude, the CMD of NGC 1755 (see Fig. 1a) shows a clear gap between the red MS and bluer stars. We start the isochrone fitting by adopting the parameters (isochrone age, distance modulus and reddening) derived in [1]. Since we are using different stellar models, we then need to adapt these parameters together with the stellar rotation parameter gradually until we obtain a pair of isochrones with the same age, but with

different initial rotational velocities that can simultaneously best match the red MS and the blue MS bands, by visual inspection. We find that stellar models with $W_i = 0.65$ and $W_i = 0.35$ can fit the observed red and blue MSs equally well in all the clusters analyzed here (see Fig. 1b and Supplementary Figure 1). The adopted parameters in the isochrone fitting, as well as the mass of the studied clusters provided in [1] are listed in Supplementary Table 1. The adopted parameters in our work are slightly different from [1], as a consequence of different employed stellar models, with slightly different initial chemical composition and adopted physics parameters. The resulting small differences in the fit parameters of the employed isochrone are not significant, because only the relative distance between red and blue isochrone well below the turn-off is important for our analysis. The bluer isochrone identifies the bulk of blue MS stars to the blue of the red isochrone, with, however, more and more stars falling to its blue side with higher brightness.

The stars to the red (right) side of the red MS are most likely unresolved close binaries, which are expected to lie in between the red MS and the corresponding equal-mass binary line, constructed by adding 0.75 magnitudes to the isochrone fitting the red MS, corresponding to a factor of two in flux (red dashed line in Fig. 1b and Supplementary Figure 5). This interpretation is strengthened by a rather sharp drop in stellar density to the red side of the equal-mass binary line seen in all the analyzed clusters. Since the location of this drop coincides well with the equal-mass binary isochrone derived from the red MS, we expect that most of the unresolved binaries, as most stars in these clusters generally, are rapid rotators. Redder stars are likely Be stars when near the turn-off [1], or higher order multiple systems otherwise.

We notice that the stars to the red (right) side of the red MS may also be explained by stars rotating with even faster velocities. Supplementary Figure 6 shows a comparison of isochrones derived from our single star models computed with different initial rotational rates, with the MS stars of NGC 1755. The adopted age, distance modulus and reddening are the same as in

4

Fig. 1b. We see that the faster rotating stellar models are redder than the slower rotating ones, due to their lower effective gravity. For slow rotation, an increase of the rotation parameter W_i by 0.1 has only a small effect on the isochrone color. However, it becomes progressively larger for faster rotation. The isochrone of our fastest rotating models ($W_i = 0.75$) overlaps the CMD region populated by suspected unresolved binaries (with large mass ratios). However the majority of the stars redder than the red MS cannot be interpreted as extremely fast rotating stars, otherwise it contradicts the observed rotational velocity distributions of the B-type and A-type stars [6, 7, 8] and the fact that Hα emitters have only been detected in the region within two magnitudes below the turn-off [1].

Supplementary Figure 6 can also be used to constrain the width of the rotational velocity distribution of the stars on the red MS. Its broadening can be delineated well by single stars with W_i from 0.45 to 0.65. Even though binaries composed of two slow rotators can also occupy the red MS, we do not expect them to play an important role if most slow rotators originate from binary mergers, after which most of them should be single stars. Nevertheless, low-mass ratio tidally-locked binaries may provide a small contribution to the red MS population (see Supplementary Information C and Supplementary Figure 8).

The choice of the rotation parameter for the isochrone fitting of the red MS is slightly degenerate, such that slightly smaller rotation parameters may also provide acceptable fits. We investigate how a different choice of W_i would impact our conclusion for the four clusters in Supplementary Figure 7. The adopted parameters are listed both in the figure and in Supplementary Table 1. Even though rotation parameters of $W_i = 0.55$ and $W_i = 0.15$ can retrieve the observed color split of the red and blue MS equally well compared to the values of $W_i = 0.65$ and $W_i = 0.35$, the former lead to several stars being bluer than the zero-age MS line in NGC 1755, NGC 330 and NGC 1818, which could not be interpreted by stellar rejuvenation caused by binary mergers. Notably, the remaining degeneracy of the rotation parameter and age for the

Supplementary Table 1: Basic information of the studied clusters and the parameters adopted in fitting the observed red and blue main sequences with our single star models. The information of the cluster mass is from [1].

Cluster	Galaxy	$\log(M/M_\odot)$	W_i for red MS	W_i for blue MS	Age (Myr)	$(m - M)_0$	$E(B - V)$
NGC 330	SMC	4.61	0.65	0.35	40	18.85	0.079
NGC 1818	LMC	4.41	0.65	0.35	40	18.31	0.067
NGC 1755	LMC	3.60	0.65	0.35	58	18.29	0.140
NGC 2164	LMC	4.18	0.65	0.35	85	18.32	0.103
NGC 330	SMC	4.61	0.55	0.15	30	18.82	0.110
NGC 1818	LMC	4.41	0.55	0.15	35	18.32	0.096
NGC 1755	LMC	3.60	0.55	0.15	48	18.28	0.177
NGC 2164	LMC	4.18	0.55	0.15	85	18.28	0.125

isochrone fitting does not affect our main conclusions, because it is not the precise values of these two parameters, but the gap in the CMD which determines our results. E.g., the derived mass functions of the red and blue MS stars change only marginally for different isochrone fits (see Supplementary Information D and Supplementary Figure 13). We show in Supplementary Information E that our conclusion of a high frequency of stellar merger events during the early cluster evolution also holds for different isochrone fits.

While it is not in the focus of this work, it is worth mentioning that the bi-modal distribution of rotation rates as adopted here is well suited to lead to an extended main sequence turn-off as it is observed in most of the young open clusters. While binary evolution is known to also contribute substantially [9], an initial rotational velocity of around 50% of critical is large enough to considerably widen the turn-off region (see Supplementary Information C and Fig. 3). The reason is that MS stars increase the ratio of rotation to critical rotation velocity during their evolution [10, 11], such that the extended main sequence turn-off will be significantly enhanced by the inclination dependence of gravity darkening.

C: Distribution of the detailed binary models in the CMD

In the main text, we have proposed that single and binary stars in young star clusters are born with nearly the same velocities with values slightly larger than half of their break-up velocities. In this section, we examine the distribution of our detailed binary models in the CMD, attempting to inspect the contribution of binary evolution to blue MS stars.

In Fig. 3, we show the CMD distribution of our binary models and binary-evolutionary products at 30 Myr. The magnitude of each binary model is obtained by adding the fluxes of the two components in the corresponding filter bands. The effect of gravity darkening is implemented according to [12, 13] by assuming a random orientation for the rotational axis of a star model. We assume that the orbit and spin vectors have the same orientation. We assign an additional shift to each binary model (or binary merger product) in the CMD by considering a Gaussian distribution for the photometric errors at the corresponding magnitudes. For comparison, we overplot the observed MS stars in NGC 330. We do not normalize the total number of our binary models to the observed number of stars, because a concrete quantitative comparison between our binary models and the observations is beyond the scope of this work.

In agreement with [9], we see in Fig. 3 that MS mergers produce a population of blue stragglers on the left side of the turn-off, between the zero-age MS line and the solid blue line. We find a deficit of MS merger products fainter than ~18.5 mags at this age, because the faint stars far below the turn-off hardly have time to expand and undergo mass transfer. Besides, our models predict very few MS merger products near the solid blue line, due to the same reason. Therefore, orbit decay during the early evolution of the binaries (see the main text) is mandatory to explain the observed dense distribution of the blue MS stars near the solid blue line. The modelling of this orbit decay is beyond the capabilities of current stellar evolution calculations.

Similar to the results in [9], our newly computed binary models predict a sequence of

critically-rotating stars to the red side of the turn-off region. These are the mass gainers of Case B mass transfer, which reach critical rotation and avoid tidal spin down, and likely correspond to Be stars. To account for the flux contribution from the decretion disk of these stars, we increase their red magnitude by 0.2 mags [14, 15].

In our shortest period binary evolution models, the rotation of the two components is affected by tides after the zero-age MS. Fig. 3 shows a population of tidally-braked binary models, in which the two stars rotate at velocities lower than their initial values. Such systems, if they have small mass ratios, may be located in positions in the CMD that we assign to hold blue MS stars. Additionally, some of our binary models contain a MS star and a stripped, hot helium burning star, which can also contribute to the observed blue MS stars. To explore the degree of contamination of blue MS from these binaries, we calculate the fraction of our detailed binary models (MS+MS binaries and MS+He burning star binaries) which would be classified as blue MS stars, with respect to the total number of binary models. We consider models as blue MS stars if their colors are bluer than the median color of the two isochrones shown in Fig. 3 at corresponding magnitudes. We do this calculation for our detailed binary models for ages from 15 to 100 Myr. The result is shown in Supplementary Figure 8.

We perform this analysis only for binary models which are at least one magnitude below the cluster turn-off, since blue and red MSs become undistinguishable near the turn-off (Fig. 3). This happens because the isochrone in this region is almost vertical, and as a consequence, the unresolved binaries (with whatever rotation) may be bluer than their single counterparts and contribute to the blue MS stars. In addition, the effect of gravity darkening is more pronounced near the turn-off, resulting in a large spread of the fast-rotating stars.

In Supplementary Figure 8, we see that for all considered ages, the fraction of binaries that contribute to blue MS stars remains below 3%, which is small compared to the fraction of the observed blue MS stars (∼20%). Also Fig. 3 shows that the majority of the tidally-braked

binaries are still found above the red MS, due to the presence of a companion, despite their slow rotation.

This result is consistent with an analysis of the initial binary parameters. According to our initial period distribution, we find that only 4.6% of the binaries hold two stars rotating at velocities lower than 15% of their critical velocities due to tides. We find that, in general, these slowly-rotating binaries can be classified as blue MS stars only if their initial mass ratios are smaller than 0.25. Assuming a flat mass ratio distribution, we conclude that only ~0.77% of the MS binaries can contaminate the blue MS stars. This simple analysis agrees well with the results in Supplementary Figure 8. Therefore, we conclude that the contribution of tidally-braked binaries to the observed blue MS stars is marginal.

D: Mass functions

In this section, we investigate the mass functions for the red and blue MS stars in the above mentioned young star clusters. We mainly employ stars between the two grey dashed, horizontal lines in the CMD figures (Fig. 1b, Supplementary Figure 5), because the red and the blue MS cannot be well distinguished either above the upper grey dashed line due to the complexity of the turn-off stars, or below the lower grey dashed line due to the large photometric errors. The blue MS stars are those marked by blue circles, while the red MS stars are those not classified as blue MS stars.

Taking NGC 1755 as an example, we plot the cumulative number distribution of the identified red and blue stars in the mass range of $5.5 \ldots 2.5 \, M_\odot$ with the solid red and blue lines in Fig. 2a and Fig. 2c. We use the mass-magnitude relation contained in the isochrones of the $W_i = 0.35$ and $W_i = 0.65$ single star models to convert the magnitude of the identified blue and red MS stars to mass. We assume that stars in each population obey a power-law mass function $N(m) \, dm \propto m^\gamma$, where m means the mass and $N(m) \, dm$ means the number of stars with masses

9

in the range m to dm. We then find the γ value that can best fit the cumulative distribution of the observed stars in each population. We do the fitting in the cumulative distribution plane to avoid the uncertainties introduced by mass bins. The results are shown with color dashed lines in Fig. 2, with the values of the mass function slopes and one sigma errors listed. One sigma error is calculated such that 68.3% of the observed distribution (solid color line) is covered, shown by the colored shaded area. The residuals that describe the difference between the observed distribution and the predicted distribution are shown in Fig. 2b and Fig. 2d for the red and the blue MS stars, respectively. We do the same for the red and the blue MS stars in the mass range of $1.8\,M_\odot$ to $2.5\,M_\odot$ in NGC 1755 and show the results in Supplementary Figure 9. It is clearly seen that even though the mass distribution of the blue MS stars smaller than $\sim 2.5\,M_\odot$ is steeper than the Salpeter IMF and the mass function of the red MS stars in the same mass range, the distribution of the higher mass blue MS stars ($> 2.5\,M_\odot$) is significantly flatter. The shallow slope for the massive blue MS stars may relate to the fact that the binary fraction is larger for more massive stars. Additionally, a shallow slope may also result from binary orbital decay simulations suggesting that binaries with higher masses are more likely to merge than binaries with lower masses [16, 17].

The derived mass function slope depends on the considered mass or magnitude range. We notice that in three of the four analysed clusters (NGC 1755, NGC 1818 and NGC 2164), the mass functions of the blue MS stars below $\sim 2.5\,M_\odot$ are steeper than a Salpeter IMF. At the same time, the split MS persists until a brightness corresponding to stars of $\sim 1.5\,M_\odot$. Nevertheless, we need to emphasise here that the distinction between the red and the blue MS stars below $\sim 2.5\,M_\odot$ becomes vague, which can be seen in Supplementary Figure 1d that the common area of the two Gaussian components is large at $m_{\mathrm{F814W}} \geq 20$. Therefore, the derived mass function for the stars less massive than $2.5\,M_\odot$ is less trustworthy than that of the more massive stars. We do not consider the stars fainter than a brightness corresponding to $\sim 2.5\,M_\odot$ in the SMC cluster

NGC 330, as the distance modulus of this cluster is larger than the three LMC clusters.

For our main result, we consider masses above $2.5\,M_\odot$. Interestingly, [7] found that in galactic field MS stars below $\sim 2.5\,M_\odot$, the slowest rotators have a significantly larger spin than above $\sim 2.5\,M_\odot$, consistent with the redder color of the blue MS stars below $\sim 2.5\,M_\odot$ in the clusters considered here. These findings may imply an intrinsic difference in star formation of the slowly-rotating stars above and below $\sim 2.5\,M_\odot$, perhaps caused by a mass dependent pre-MS evolution. Due to the lack of spectroscopic observations and the larger photometric errors for the stars below $2.5\,M_\odot$, we do not include them in our analysis. Nevertheless, the mass functions of the blue MS stars above $\sim 2.5\,M_\odot$ undoubtedly reveal a discrepancy with the Salpeter IMF, i.e. our conclusion that the red and blue MS stars have different mass functions is robust for stars whose masses are larger than $\sim 2.5\,M_\odot$.

We do the same experiment for the SMC cluster NGC 330 and the LMC clusters NGC 1818 and NGC 2164. The results are shown in Supplementary Figure 10, Supplementary Figure 11, and Supplementary Figure 12, respectively. We summarize the derived slopes and errors of the mass functions of the MS stars more massive than $2.5\,M_\odot$ in different clusters in Supplementary Table 2. Even though the error of the derived slope of the blue MS stars in NGC 2164 is large, the slope distinction between the red and blue MS stars clearly exists. We found no significant differences between the mass function slopes measured across the four clusters, thus we argue that the mass function dichotomy is ubiquitous in all the studied clusters.

To assess to what extent the derived γ values are affected by blue MS star classification, we examine different boundary lines to define the red and the blue MS stars, based on isochrone fitting. We consider boundary lines to lie on the right side of the isochrone for the blue MS, with a color difference equal to a fraction Q of the color separation between the isochrones for the red and the blue MSs. Q ranges from 0 to 1, in intervals of 0.2, with $Q = 0$ ($Q = 1$) representing the extreme case that all stars on the left side of the isochrone for the blue (red) MS

Supplementary Table 2: Slopes γ and uncertainties of the mass functions derived for the red and blue main-sequence stars with estimated masses larger than $2.5\,M_\odot$ in four clusters. The last column shows the number ratio between the blue main-sequence stars and all stars in the same mass range.

Cluster	Galaxy	γ for the red MS stars	γ for the blue MS stars	$N_{\text{blue MS}}/(N_{\text{blue MS}} + N_{\text{red MS}})$
NGC 330	SMC	-2.37 ± 0.28	0.37 ± 0.39	$0.19^{+0.18}_{-0.07}$
NGC 1818	LMC	-1.90 ± 0.20	-0.13 ± 0.31	$0.15^{+0.13}_{-0.05}$
NGC 1755	LMC	-2.17 ± 0.15	-1.03 ± 0.32	$0.18^{+0.21}_{-0.06}$
NGC 2164	LMC	-2.38 ± 0.43	0.04 ± 1.20	$0.15^{+0.23}_{-0.05}$

are assigned as blue MS stars. The stars that are not classified as blue MS stars are considered as red MS stars. We only consider the stars between the two grey dotted lines in Fig. 1 and Supplementary Figure 5. The variation of the derived γ values for the red and the blue MS stars with respect to Q in the four clusters is shown in Supplementary Figure 13. It reveals that the mass functions of the red MS stars more massive than $2.5\,M_\odot$ in all four clusters are comparable to the Salpeter IMF. While the mass functions of the blue MS stars in the same mass range in all four clusters have significantly shallower slope than the Salpeter IMF, with the slope becoming slightly steeper as we use redder boundary lines. Nevertheless, the disparity between the mass function of the blue MS stars and the Salpeter IMF exists even in an extreme case of $Q = 1$.

At last, we use the same stars as we employed in mass function estimation to calculate the fraction of the blue MS stars. The results are shown in Supplementary Table 2, with the mean values obtained by assuming $Q = 0.5$ when computing the borderline between the red and the blue MS stars, and the lower and upper errors obtained by assuming $Q = 0$ and $Q = 1$, respectively. We found that the ratio of the blue MS stars is almost identical in all four clusters.

E: Merger models and merger history

We suggest that MS mergers are responsible for the formation of the blue MS stars, according to the fact that they can produce blue stragglers [9] that appear younger than the other cluster stars. In this scenario, we can estimate the possible merger time t_{merge} of each blue MS star, which is the time in the cluster history when the merger happens, by comparing its distribution in the CMD with the theoretical merger models. We next describe in detail how we do this.

For each initial rotation, we construct a series of lines in the CMD that represent the current positions of the merger products whose progenitors coalesced at given times in the past, from 0 Myr after starburst to the age of the cluster, in intervals of 1 Myr. Supplementary Figure 14 shows some representative lines by assuming rotational velocities of 35% of the break-up velocities for the merger products. We then use the nearest line to determine t_{merge} for each observed blue MS star. The adoption of faster rotating merger models results in a larger t_{merge} for a given observed blue MS star, because faster rotating merger models are redder than the slower rotating ones with the same t_{merge}. Supplementary Figure 14 indicates that most of the observed blue MS stars above 19.5th magnitude can be covered by merger models with a rotation parameter of $W_{\mathrm{i}} = 0.35$, however, there are outliers to the right and left of the family of lines, indicating that somewhat larger or slower rotation is required for these cases. For example, the blue MS stars between the two isochrones that are used to fit the observed blue and red MS stars (see Fig. 1b) cannot be reproduced by merger models with a rotational rate smaller than 35% of their critical velocities. For those stars, we calculate the maximum and minimum rotational rates with which merger models can reach these stars in the CMD.

The derived t_{merge} for the NGC 1755 blue MS stars are shown in Fig. 4b (lower panel), with the lower limits determined by the merger models with the maximum allowed rotation and the upper limits determined by the merger models with the minimum allowed rotation. We only

13

include stars brighter than 19th magnitude, because we lose diagnostic power beyond that as the fastest rotating merger models produced at 58 Myr are bluer than the slowly rotating merger models produced at 0 Myr. We also exclude the brightest blue MS stars whose magnitudes are smaller than 15.5, because they are brighter than all our merger models. Perhaps they are extremely fast rotating stars which may be subject to strong gravity darkening/brightening. Finally, we compute the merger history by assuming a Gaussian distribution within the allowed merger velocities, with a mean value of $W_i = 0.35$ and a standard deviation of $W_i = 0.2$. This distribution is chosen because the isochrone with $W_i = 0.35$ can fit the blue MS well, and the width of this Gaussian distribution can cover all the identified blue MS stars. This leads to the merger event history of the blue MS stars of NGC 1755 as shown in Fig. 4a (upper panel). The time resolution is 1 Myr, which is governed by the t_{merge} interval used when we build the merger models. We perform a bootstrapping analysis to obtain the uncertainty of the derived merger time distribution. We randomly assign a rotational velocity for each blue MS star following a Gaussian distribution, and derive its corresponding merger time. We repeat this process 10 000 times, and determine the 1σ uncertainty as the place where 68% of the 10 000 obtained number of mergers per Myr is included in each t_{merge} bin. The result is shown by the shaded area in Fig. 4a. Our results reveal that merger events should be prevalent in the first tens of Myrs, with a peak at 0 Myr to 2 Myrs, to account for the many observed stars near the blue MS.

The distribution of the blue MS stars in the CMD indicates an earlier merger time for brighter stars (see the blue MS stars with magnitudes between 16.5 and 18 near the $t_{merge} = 0$ line in Supplementary Figure 14). In order to examine the correlation between the derived merger time and magnitude, we calculate the Spearman's rank correlation coefficient between these two variables in all 10 000 bootstrapping simulation. The obtained coefficient ranges from 0.38 to 0.60, with an average value of 0.50, indeed indicating a moderate positive correlation. Such a correlation may be consistent with the results of recent binary orbit decay simulations,

which propose that more massive binaries are expected to merge earlier than binaries with lower massive stars due to their larger angular momentum and energy loss rates caused by dynamical friction [16].

In order to check whether the derived merger rate history is affected by our isochrone fitting, we do the same experiment using the isochrones shown in Supplementary Figure 7. The results are shown in Supplementary Figure 15. This time, we consider the merger products to have 0 to 45% of their critical velocities, following a Gaussian distribution with a peak at $W_i = 0.15$ and a width of $W_i = 0.3$. These values are chosen such that the rotation peak matches the rotation of the single star models that are used to fit the blue MS, and all blue MS stars are covered, except for several stars which fall on the blue side of the zero-age MS line in Panel a of Supplementary Figure 7. The rise of the merger event rate at recent times in Supplementary Figure 15 is caused by ample blue MS stars that can only be reached by non/slowly rotating mergers formed very recently. These blue MS stars have smaller derived rotational rates and t_{merge} range, thus a larger probability in each allowed t_{merge} bin. However, our main conclusion that merger events are prevalent in the first tens of Myr remains intact. The Spearman's rank correlation coefficient in this case is 0.59.

We use the same method to estimate the merger history of the blue MS stars in the SMC cluster NGC 330 and the LMC clusters NGC 1818 and NGC 2164, with the results shown in Supplementary Figure 16. The isochrone fitting is done by employing $W_i = 0.65$ and $W_i = 0.35$ models. We see that our conclusion that mergers happen frequently in the first tens of Myr holds in all the studied clusters. Besides, the derived merger event frequencies in these three clusters all show a continuously decreasing trend. The mean derived Spearman's rank correlation coefficients are 0.20, 0.59 and 0.48 for clusters NGC 330, NGC 1818 and NGC 2164, respectively, all implying a moderate positive correlation between the derived merger time and magnitude.

In the above analysis, we only consider binary mergers from equal-mass binaries, which possess the strongest rejuvenation. In the following, we examine how the mass ratio of the merger progenitors affects our results. We first quantify the relation between the apparent rejuvenation (how much younger the star looks than it really is) and the mass ratio. We describe the apparent rejuvenation as $(t - t_{app})/t$, where t is the time at which a merger happens, and t_{app} is the apparent age of the merger product. We consider binaries with primary masses between 2.1 $M_\odot$ and 10 $M_\odot$ in intervals of 0.5 $M_\odot$, and mass ratios between 0.2 and 1 in intervals of 0.2. We assume mergers happen at 58 Myr (i.e., the derived age of cluster NGC 1755), and show the result in Supplementary Figure 17. It can be seen that rejuvenation increases with increasing mass ratio. For example a 5 $M_\odot$ merger product can be rejuvenated to $\sim 40\%$ and $\sim 80\%$ younger than its progenitors if it is produced by a $q = 0.2$ and a $q = 1$ binary, respectively. In order to perform this examination, we extend our single star models to 0.4 $M_\odot$. But we only build and use the zero-age MS models for such low-mass stars, as they hardly evolve in young star clusters.

We show the distribution of our merger products created at 58 Myr from binaries with different mass ratios in the CMD in Supplementary Figure 18, and the resulting merger history in Supplementary Figure 19. We only include blue MS stars that can be covered by our merger models in this check. It leads to different integral number of the derived merger events under the assumption of different mass ratios. The merger models constructed with low mass ratios are redder in the CMD compared to their high mass-ratio counterparts, thus can cover fewer observed blue MS stars. In Supplementary Figure 18 and Supplementary Figure 19, we see that results for mass ratios larger than 0.6 are nearly identical. The rate of the merger events increases after ~ 54 Myr when adopting mass ratios smaller than 0.4, because more blue MS stars have smaller derived rotational rate and merger time ranges. Nevertheless, our main conclusion that merger events should occur at early times is robust, regardless of the binary mass ratio.

16

Apart from the above-mentioned uncertainties, the derived merger times may also be affected by additional mixing during the merger process, which can make a merger product appear even younger (1.14 times for stars above $5\,M_\odot$ and 1.43 times for stars below $5\,M_\odot$) than in the case of fully rejuvenation [18, 19]. However, this additional mixing does not significantly affect the distribution of early mergers in the CMD, as the long-lasting later evolution of the merger product after it has been created washes out this small natal difference. Whereas potential surface He enhancement may also impact the distribution of the merger products, it is not found in both theoretical simulations or spectroscopic observations [20, 19, 21].

We have proposed in the main text that orbital decay in multiple systems happens probably via Kozai-cycles. A glimpse of the MS distribution in the CMD at the present clusters gives us the impression that there are many suspected triples or higher-order multiples (see Fig. 1b and Supplementary Figure 5, those with colors redder than the equal-mass binary line red shifted by three times the photometric error). To indicate this, we derive the fraction of the suspected triple or higher-order multiples with respect to all MS stars in three clusters, one SMC cluster NGC 330, and two LMC clusters, NGC 1818 and NGC 1755. In figures comparing our theoretical isochrones with the observations in the CMD (Fig. 1b and Supplementary Figure 5), we count the stars on top of the equal-mass binary lines shifted redwards by three times the photometric errors as the suspected triple or higher-order multiples. The results are shown in Supplementary Figure 20. We use absolute magnitude such that we can directly compare clusters with different ages in different galaxies. We use isochrones of $W_i = 0.65$ single star models that can best fit the red MS in each cluster to convert the apparent magnitude to the absolute magnitude. We consider stars whose absolute magnitudes are 2 mags larger than the turn-off magnitude to exclude the probable contaminations from critically rotating Be stars. At the low-brightness end, we cut at $M_{F814W} = 2$, which roughly corresponds to an apparent magnitude of 20.5 in these clusters. We show our results in different magnitude intervals. The error bars on

the x-axis reflect the magnitude intervals, while the error bars on the y-axis reflect the Poisson error. In general, the fraction of the suspected triples decreases with increasing magnitude. We point out that these values should only be the lower limit, as we miss the low mass ratio multiple systems whose positions are below the boundary lines.

References

[1] Milone, A. P. *et al.* Multiple stellar populations in Magellanic Cloud clusters - VI. A survey of multiple sequences and Be stars in young clusters. *Mon. Not. R. Astron. Soc.* **477**, 2640–2663 (2018). `1802.10538`.

[2] Milone, A. P. *et al.* Multiple stellar populations in Magellanic Cloud clusters - IV. The double main sequence of the young cluster NGC 1755. *Mon. Not. R. Astron. Soc.* **458**, 4368–4382 (2016). `1603.03493`.

[3] Bastian, N. & de Mink, S. E. The effect of stellar rotation on colour-magnitude diagrams: on the apparent presence of multiple populations in intermediate age stellar clusters. *Mon. Not. R. Astron. Soc.* **398**, L11–L15 (2009).

[4] Niederhofer, F., Georgy, C., Bastian, N. & Ekström, S. Apparent age spreads in clusters and the role of stellar rotation. *Mon. Not. R. Astron. Soc.* **453**, 2070–2074 (2015). `1507.07561`.

[5] Correnti, M., Goudfrooij, P., Bellini, A., Kalirai, J. S. & Puzia, T. H. Dissecting the extended main-sequence turn-off of the young star cluster NGC 1850. *Mon. Not. R. Astron. Soc.* **467**, 3628–3641 (2017). `1612.08746`.

[6] Huang, W., Gies, D. R. & McSwain, M. V. A Stellar Rotation Census of B Stars: From ZAMS to TAMS. *Astrophys. J.* **722**, 605–619 (2010). `1008.1761`.

[7] Zorec, J. & Royer, F. Rotational velocities of A-type stars. IV. Evolution of rotational velocities. *Astron. Astrophys.* **537**, A120 (2012). `1201.2052`.

[8] Dufton, P. L. *et al.* The VLT-FLAMES Tarantula Survey. X. Evidence for a bimodal distribution of rotational velocities for the single early B-type stars. *Astron. Astrophys.* **550**, A109 (2013). `1212.2424`.

[9] Wang, C. *et al.* Effects of Close Binary Evolution on the Main-sequence Morphology of Young Star Clusters. *Astrophys. J. Lett* **888**, L12 (2020). `1912.07294`.

[10] Ekström, S., Meynet, G., Maeder, A. & Barblan, F. Evolution towards the critical limit and the origin of Be stars. *Astron. Astrophys.* **478**, 467–485 (2008). `0711.1735`.

[11] Hastings, B., Wang, C. & Langer, N. The single star path to Be stars. *Astron. Astrophys.* **633**, A165 (2020). `1912.05290`.

[12] Espinosa Lara, F. & Rieutord, M. Gravity darkening in rotating stars. *Astron. Astrophys.* **533**, A43 (2011). `1109.3038`.

[13] Paxton, B. *et al.* Modules for Experiments in Stellar Astrophysics (MESA): Pulsating Variable Stars, Rotation, Convective Boundaries, and Energy Conservation. *Astrophys. J. Supp.* **243**, 10 (2019). `1903.01426`.

[14] Labadie-Bartz, J. *et al.* Photometric Variability of the Be Star Population. *Astron. J.* **153**, 252 (2017). `1609.08449`.

[15] Hastings, B., Langer, N., Wang, C., Schootemeijer, A. & Milone, A. P. A stringent upper limit on Be star fractions produced by binary interaction. *arXiv e-prints* arXiv:2106.12263 (2021). `2106.12263`.

[16] Korntreff, C., Kaczmarek, T. & Pfalzner, S. Towards the field binary population: influence of orbital decay on close binaries. *Astron. Astrophys.* **543**, A126 (2012). `1205.6311`.

[17] Tokovinin, A. & Moe, M. Formation of close binaries by disc fragmentation and migration, and its statistical modelling. *Mon. Not. R. Astron. Soc.* **491**, 5158–5171 (2020). `1910.01522`.

[18] Glebbeek, E. & Pols, O. R. Evolution of stellar collision products in open clusters. II. A grid of low-mass collisions. *Astron. Astrophys.* **488**, 1017–1025 (2008). `0806.0865`.

[19] Glebbeek, E., Gaburov, E., Portegies Zwart, S. & Pols, O. R. Structure and evolution of high-mass stellar mergers. *Mon. Not. R. Astron. Soc.* **434**, 3497–3510 (2013). `1307.2445`.

[20] Sills, A., Faber, J. A., Lombardi, J., James C., Rasio, F. A. & Warren, A. R. Evolution of Stellar Collision Products in Globular Clusters. II. Off-Axis Collisions. *Astrophys. J.* **548**, 323–334 (2001). `astro-ph/0008254`.

[21] Carini, R., Biazzo, K., Brocato, E., Pulone, L. & Pasquini, L. MUSE Observations of NGC330 in the Small Magellanic Cloud: Helium Abundance of Bright Main-sequence Stars. *Astron. J.* **159**, 152 (2020). `2002.02906`.
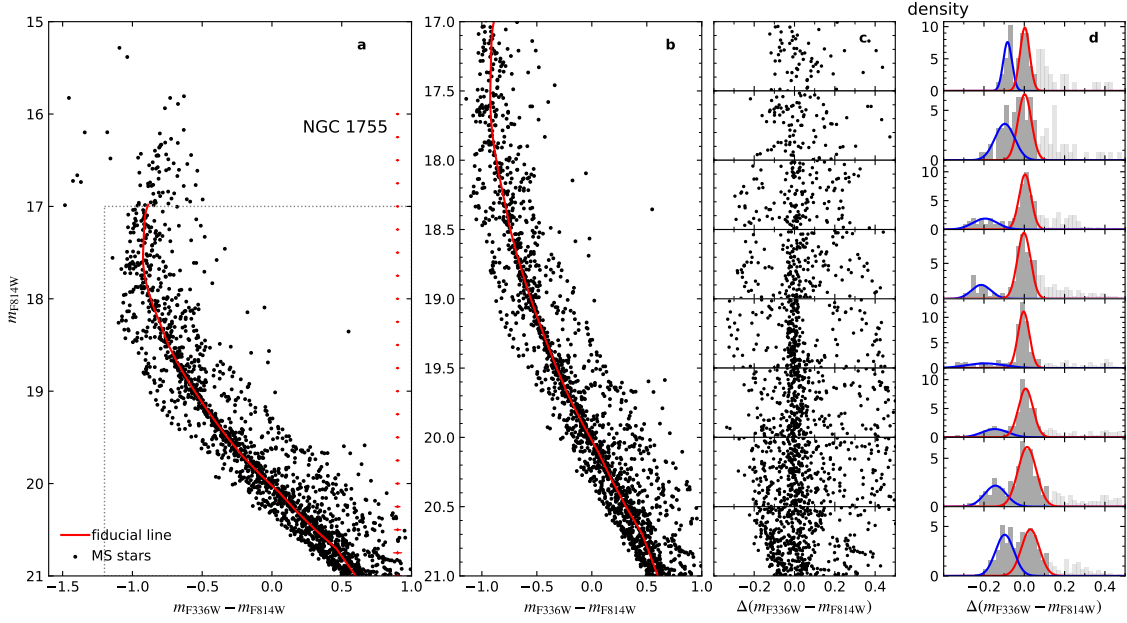
Supplementary Figure 1: Distinguishing red and blue main-sequence stars in NGC 1755. **a**: Same as Fig. 1a, but with a fiducial line (solid red line) that best describes the distribution of the red main-sequence stars. The stars in the region delineated by the grey dotted lines are considered in this procedure. The red error bars on the right indicate 1σ error at corresponding magnitudes. **b**: Zoom-in image of the area delineated by the grey dotted lines in panel a. **c**: Horizontal color distance $\Delta(m_{F336W} - m_{F814W})$ of each star in panel b to the fiducial line as a function of magnitude. **d**: Histogram distribution of the points in panel c in corresponding magnitude intervals. The dark grey (light grey) histograms are included (excluded) in our bi-Gaussian fitting. The dark grey histograms are normalized such that their total area equals one, while the light grey histograms are normalized such that their total area equals the number ratio of the stars excluded and included in our bi-Gaussian fitting. The red and blue curves depict the components of our best bi-Gaussian fitting for the dark grey histograms. The stars with $\Delta(m_{F336W} - m_{F814W})$ smaller than that of the cross of the red and blue curves are identified as blue MS stars.

21
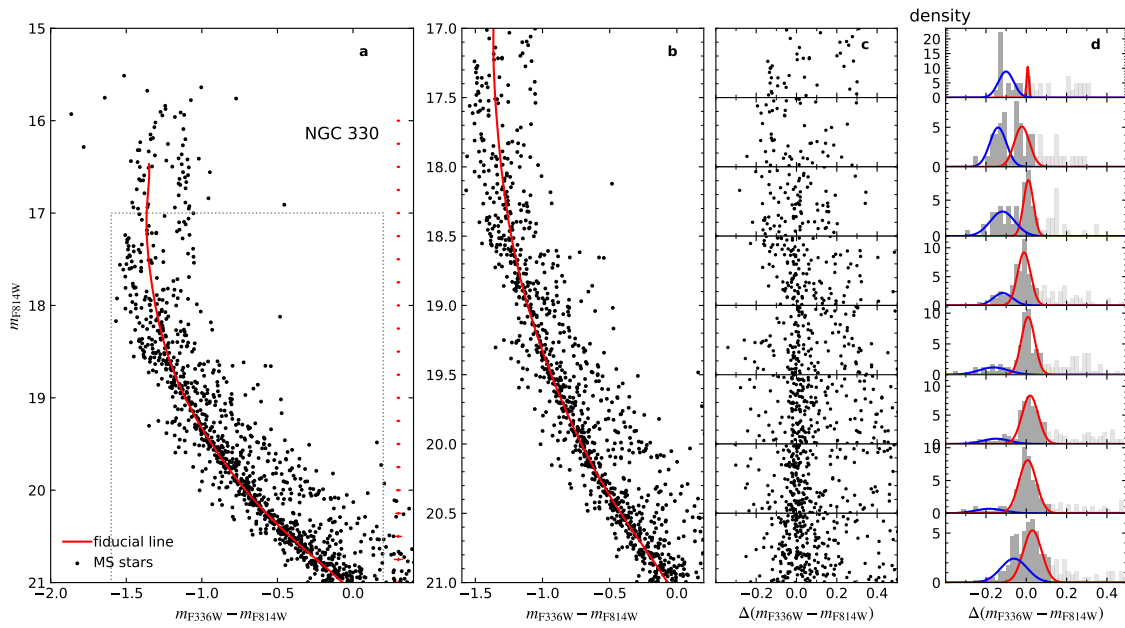
Supplementary Figure 2: Same as Supplementary Figure 1, but for distinguishing the red and the blue main-sequence stars in NGC 330.
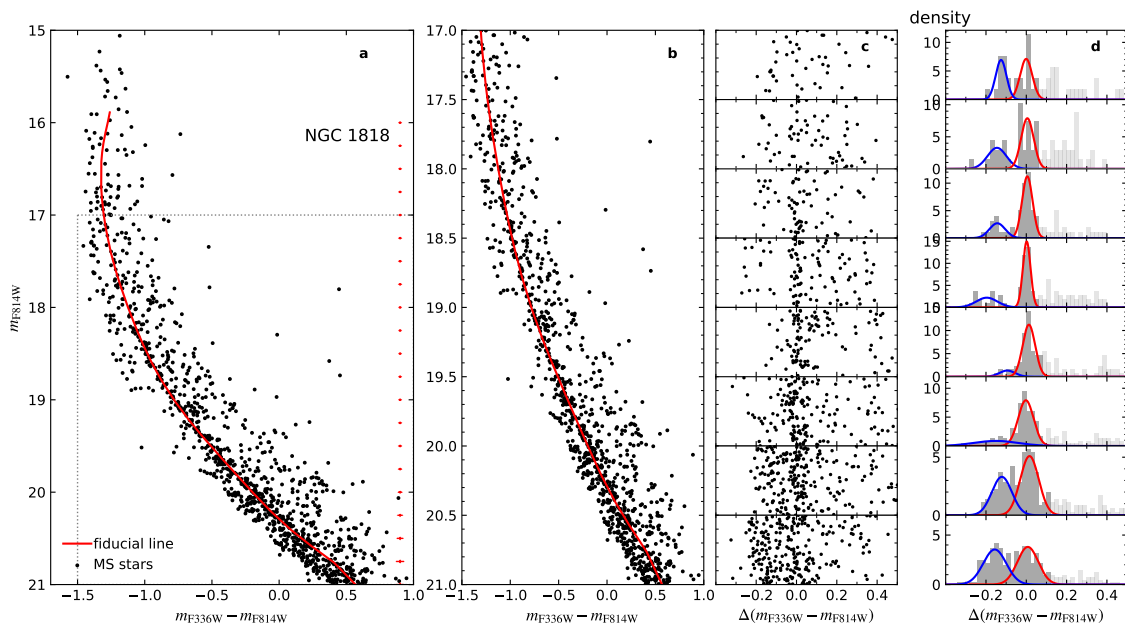
Supplementary Figure 3: Same as Supplementary Figure 1, but for distinguishing the red and the blue main-sequence stars in NGC 1818.
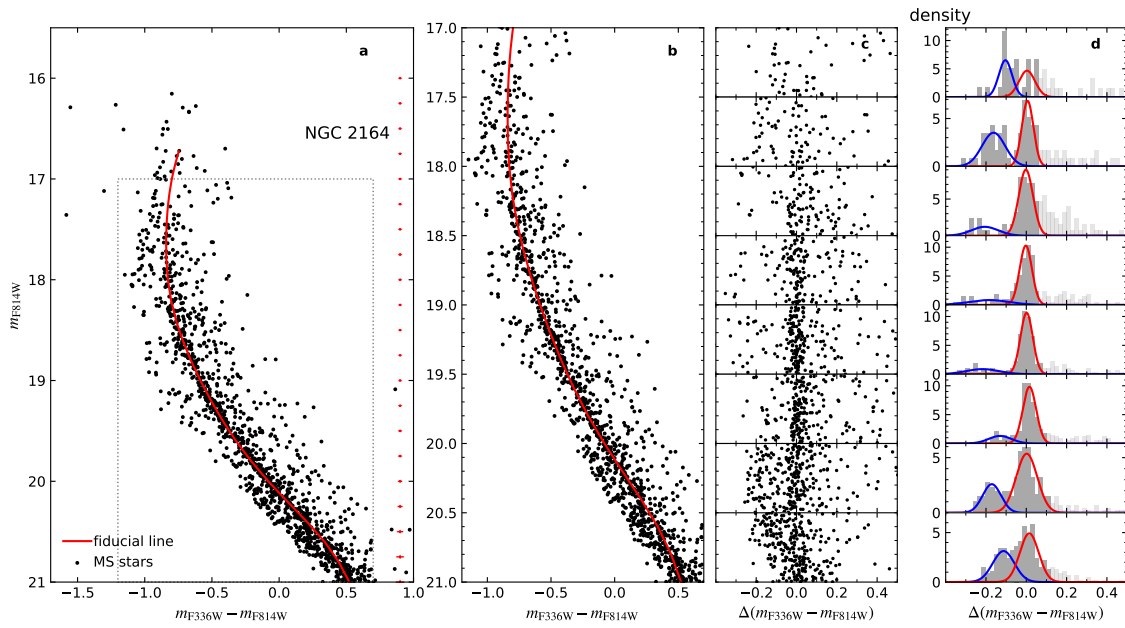
Supplementary Figure 4: Same as Supplementary Figure 1, but for distinguishing the red and the blue main-sequence stars in NGC 2164.
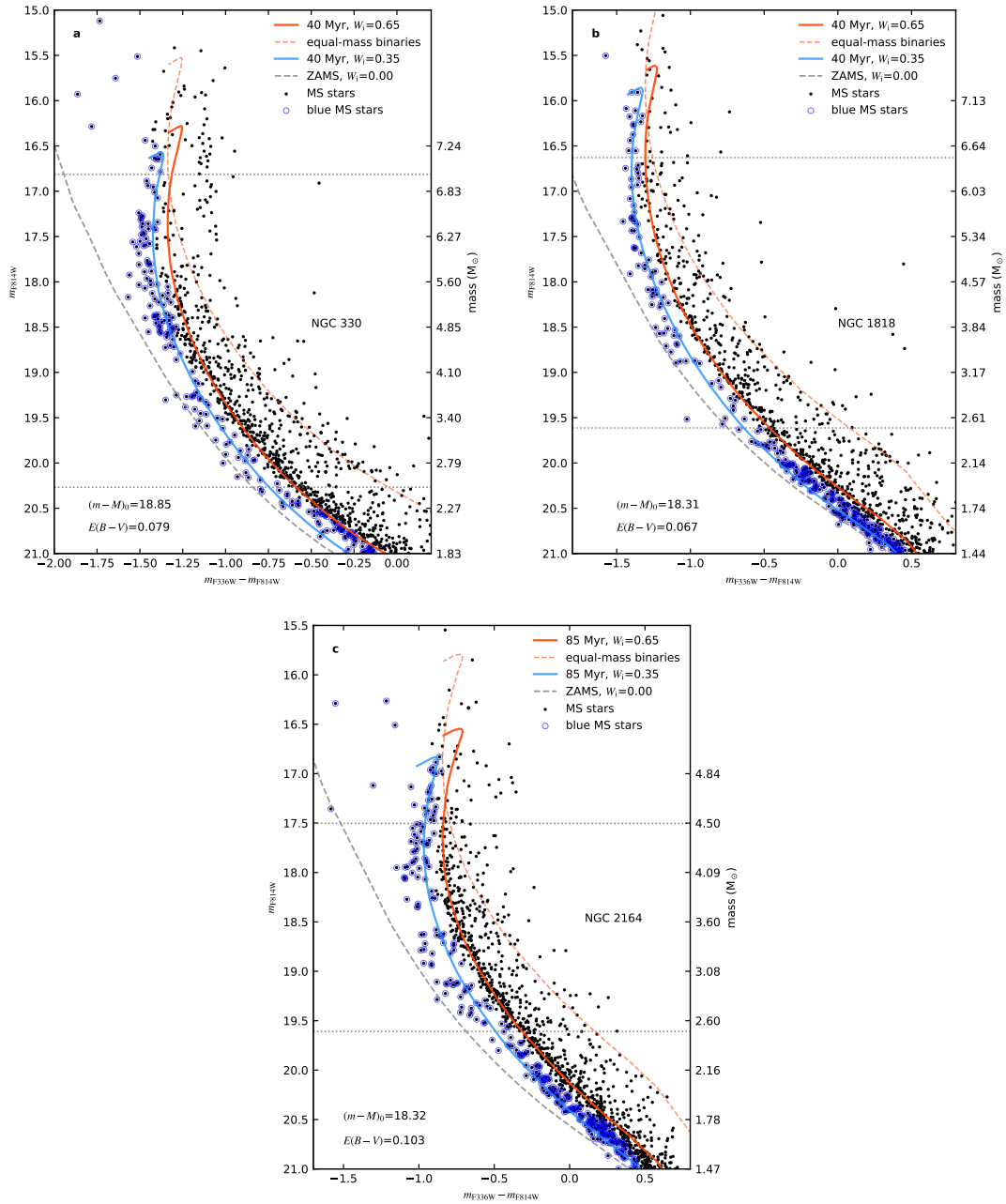
Supplementary Figure 5: Isochrone fits to the main-sequence stars in three young star clusters. The plots are the same as Fig. 1b. The adopted distance moduli and reddenings are indicated (see also Supplementary Table 1).
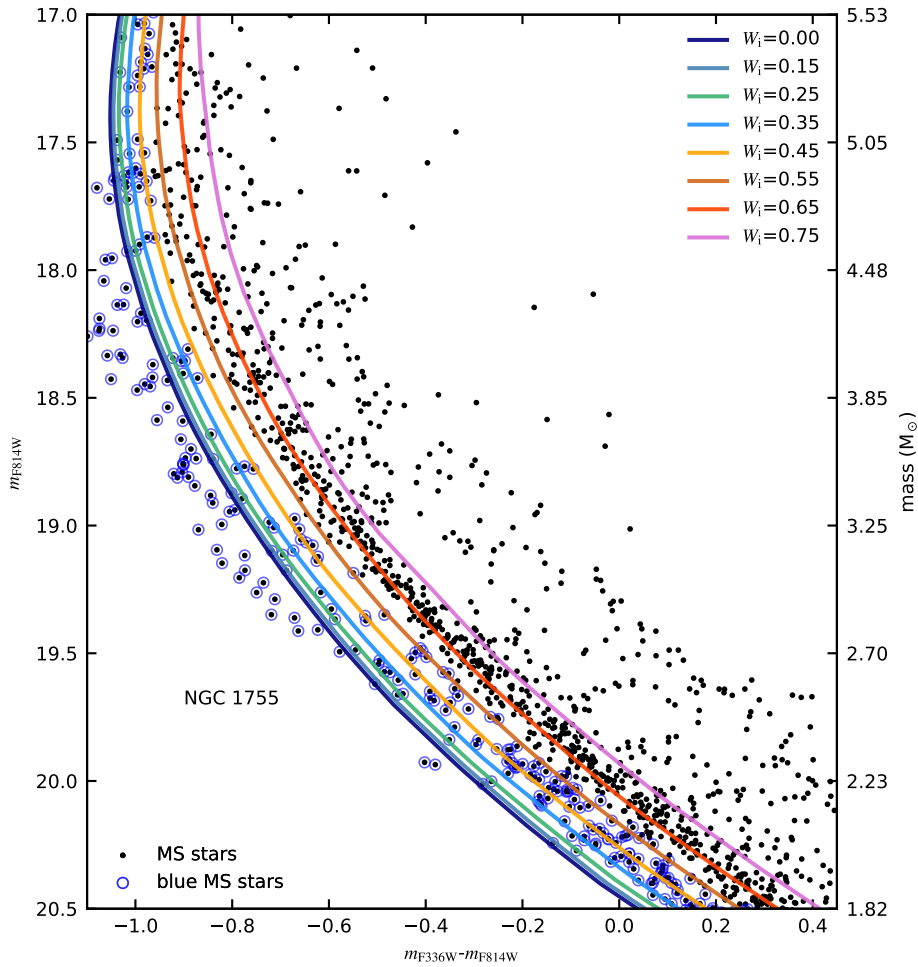
Supplementary Figure 6: Effect of rotation on the color of main-sequence stars. The black dots and blue open circles correspond to the observed main-sequence stars and the identified blue main-sequence stars in NGC 1755, respectively. The isochrones are derived from our single star models with different initial rotational rates, as indicated in the legend. The adopted distance modulus and reddening are the same as Fig. 1b, as are the isochrones with a rotation parameter of $W_i = 0.35$ and $W_i = 0.65$. The right y-axis displays the stellar masses derived from the mass-magnitude relation of the models with 65% of critical rotation initially.
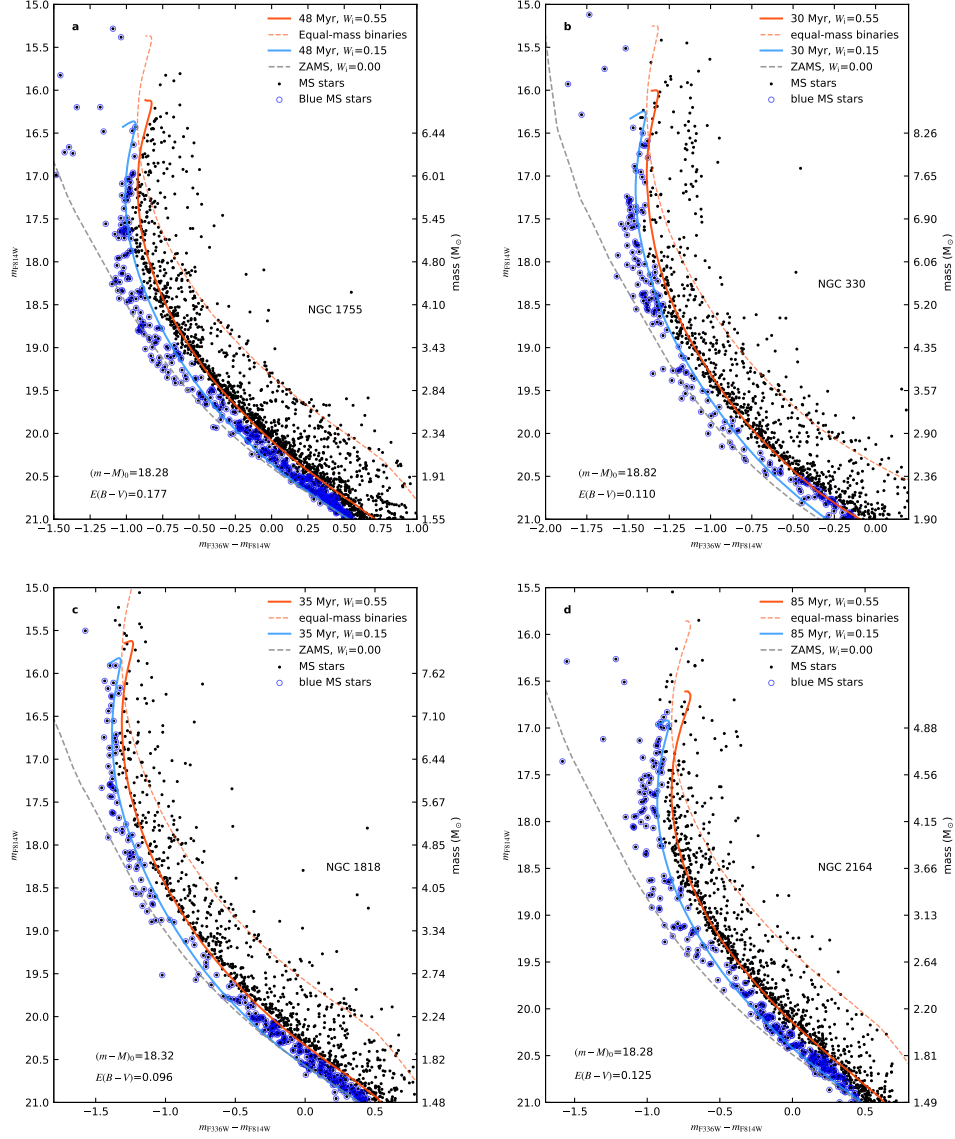
Supplementary Figure 7: Isochrones for four young star clusters using alternative stellar rotation. The plots are the same as Fig. 1b, but stellar models with different initial rotational velocities ($W_i = 0.55$ and $W_i = 0.15$) are employed to fit the red and blue main-sequences of the clusters (see legends). The adopted distance moduli and reddenings are indicated both in the figure and in Supplementary Table 1.
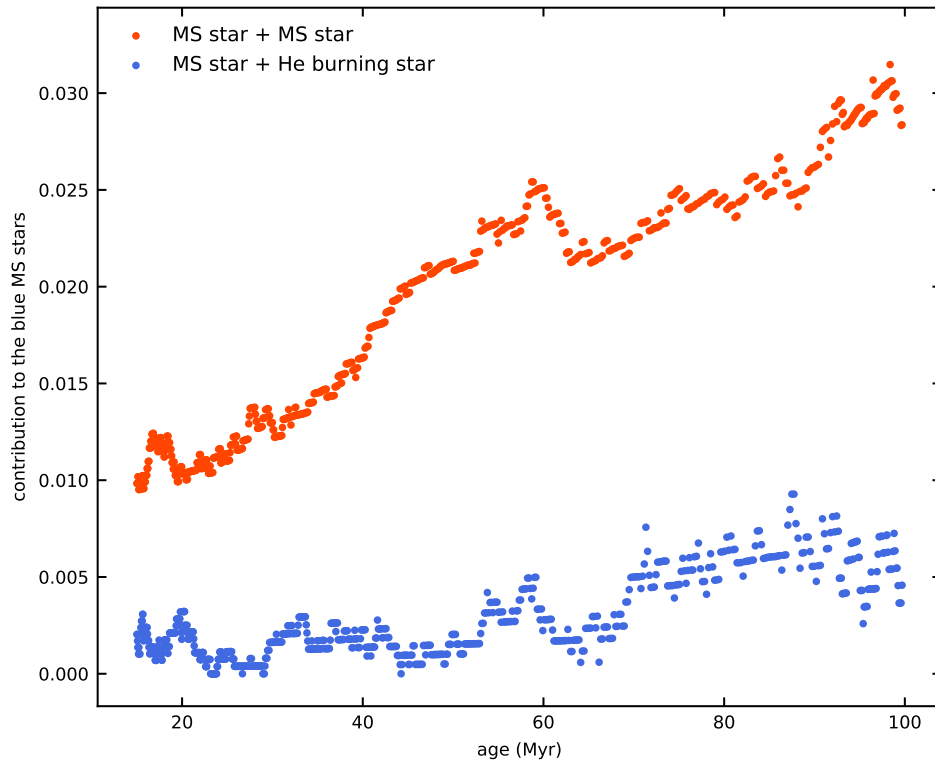
Supplementary Figure 8: Contribution of binaries (non-mergers) to the blue main-sequence for different ages. Red and blue dots correspond to the fraction of binary models containing two main-sequence stars and binary models containing a main-sequence star and a He burning star, that will be classified as blue main-sequence stars, with respect to all the binary models, respectively.
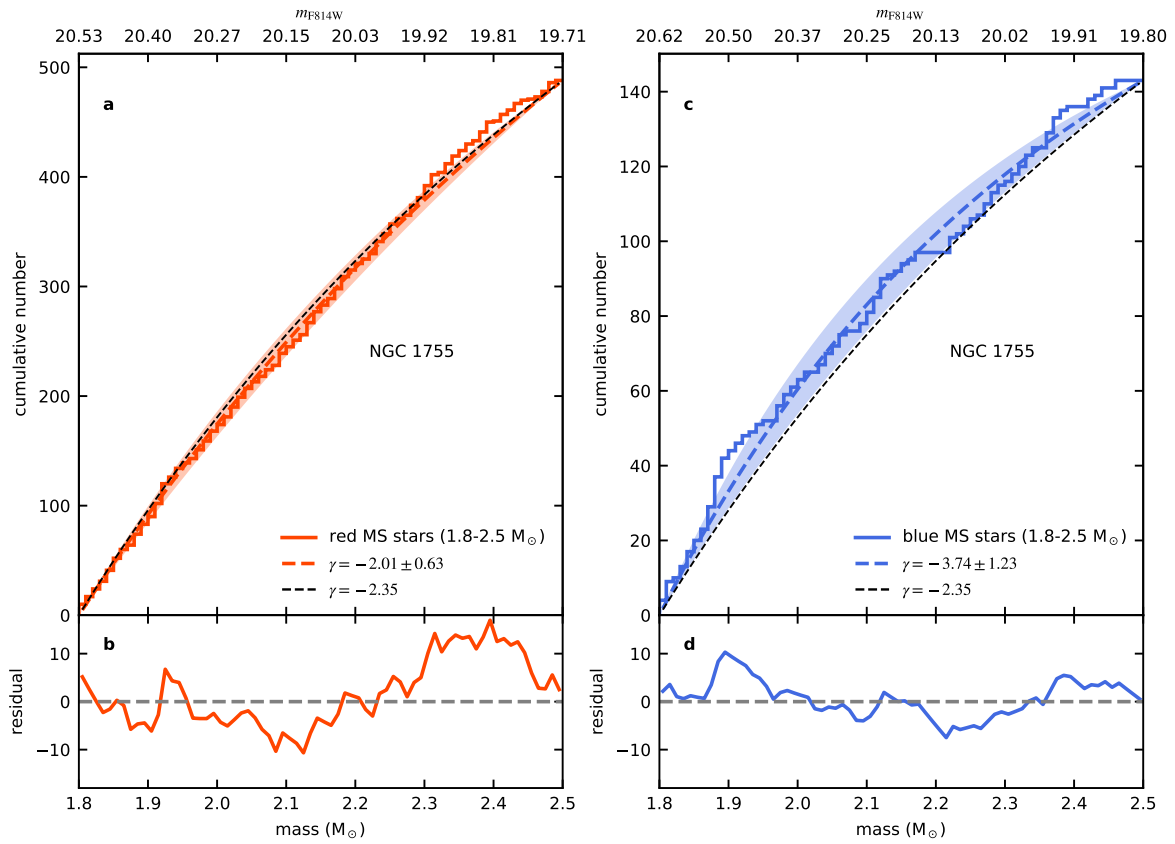
Supplementary Figure 9: Mass function of the low-mass red and blue main-sequence stars in NGC 1755. The plots are the same as Fig. 2. The considered mass range is 1.8 to 2.5 $M_\odot$.
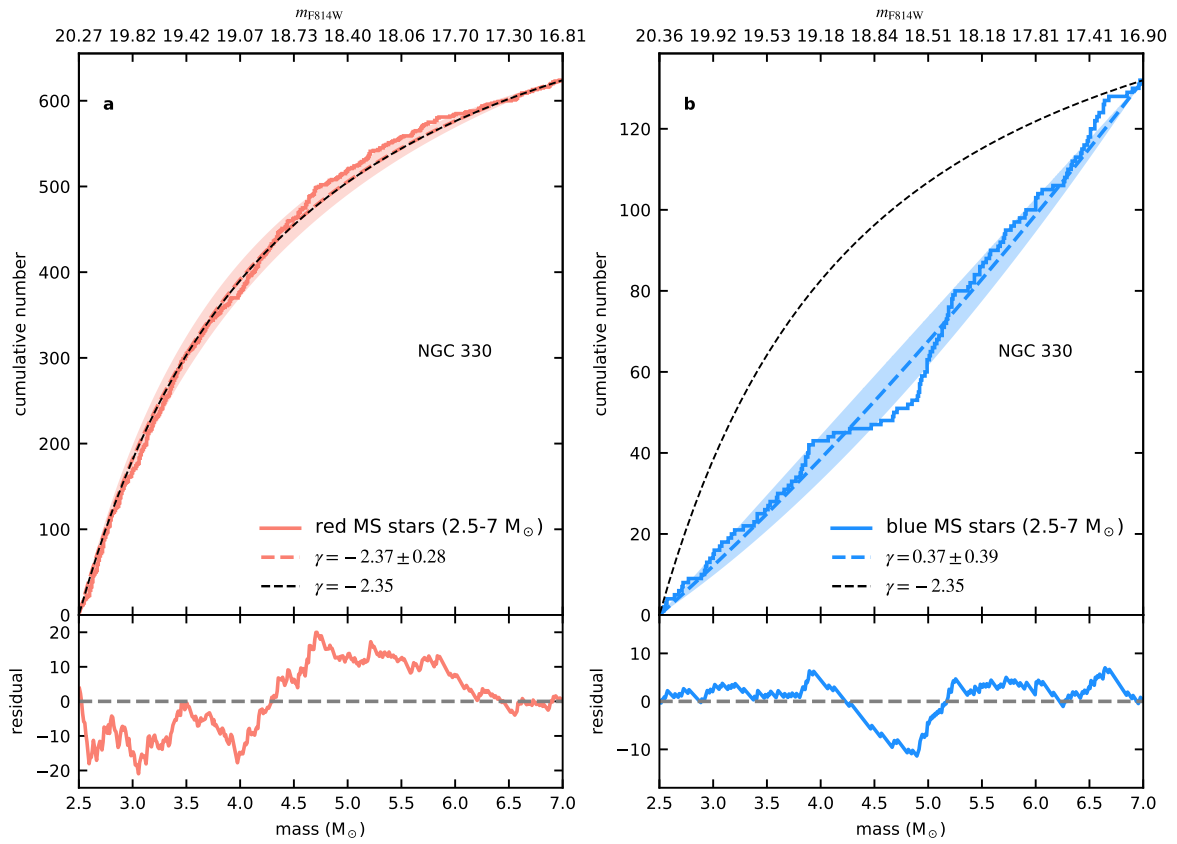
Supplementary Figure 10: Mass function of the red and the blue main-sequence stars in NGC 330. The plots are the same as Fig. 2. Only the stars with derived masses larger than $2.5\,\mathrm{M_\odot}$ are considered.
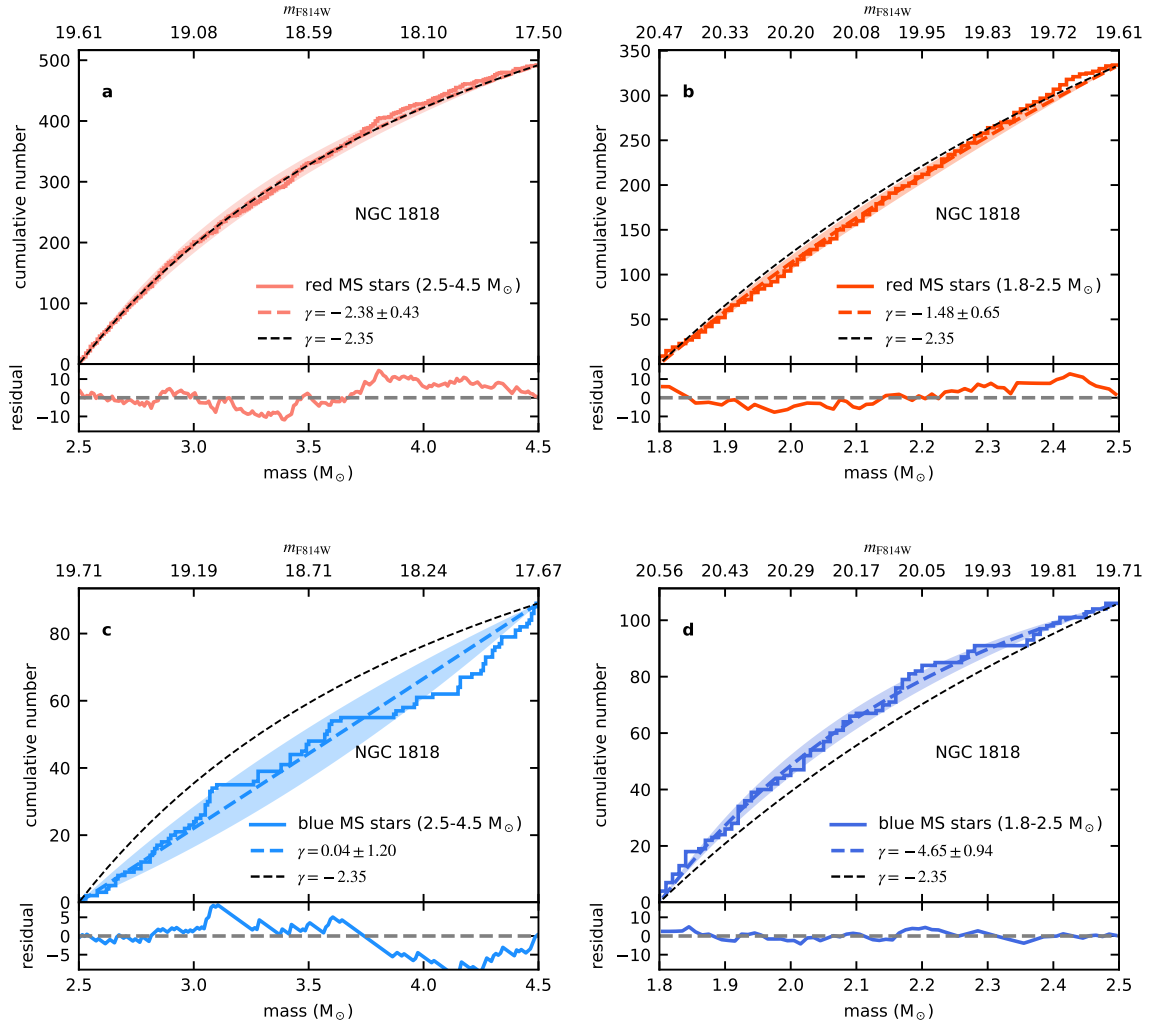
Supplementary Figure 11: Mass function of the red and the blue main-sequence stars in NGC 1818. Panels a and c correspond to the results of the red and the blue MS stars in the mass range of 2.5 to 6.5 M$_\odot$, respectively. While Panels b and d show the results of the red and the blue MS stars in the mass range of 1.8 to 2.5 M$_\odot$, respectively.
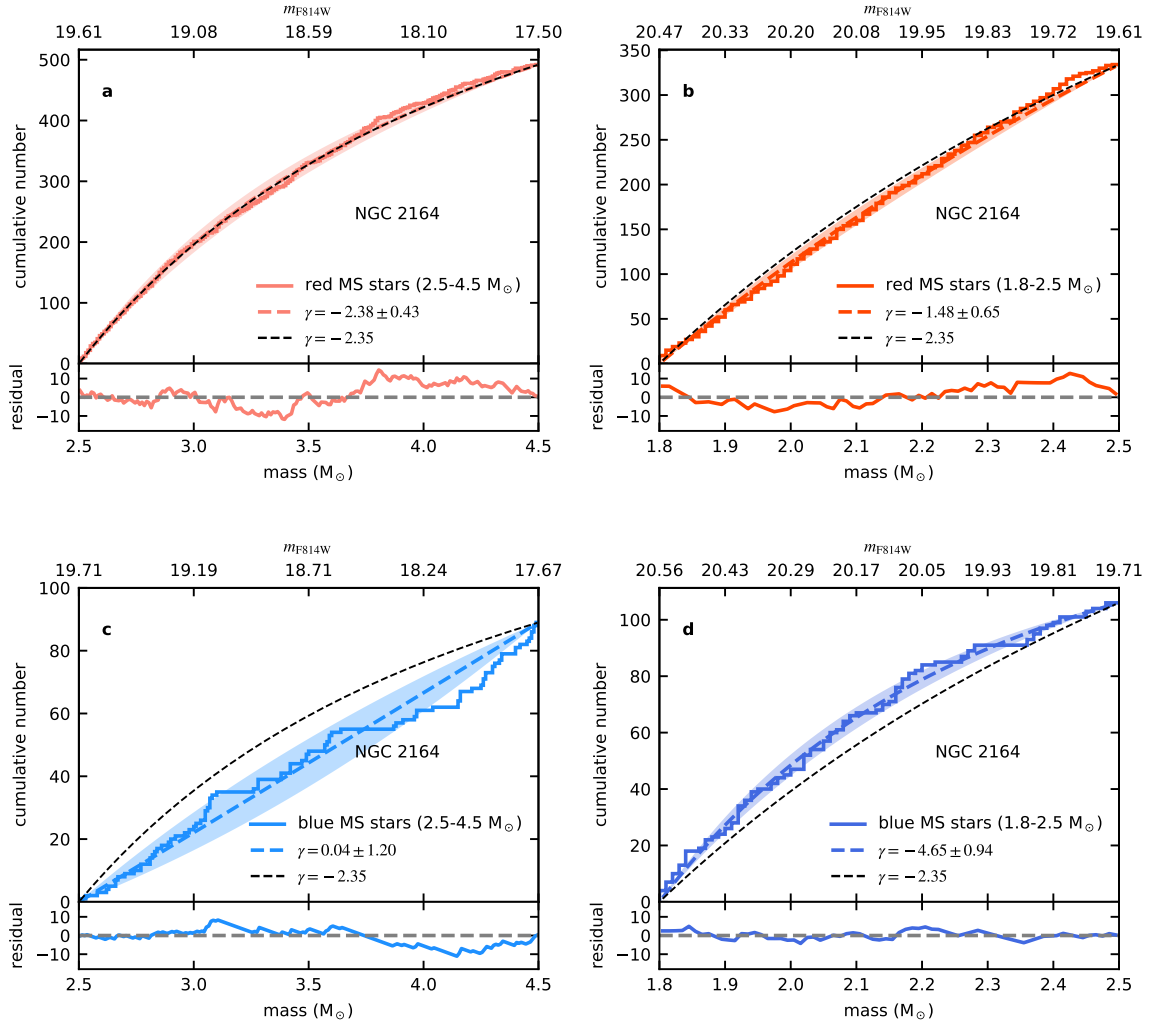
Supplementary Figure 12: Mass function of the red and the blue main-sequence stars in NGC 2164. The plots are the same as Supplementary Figure 11.
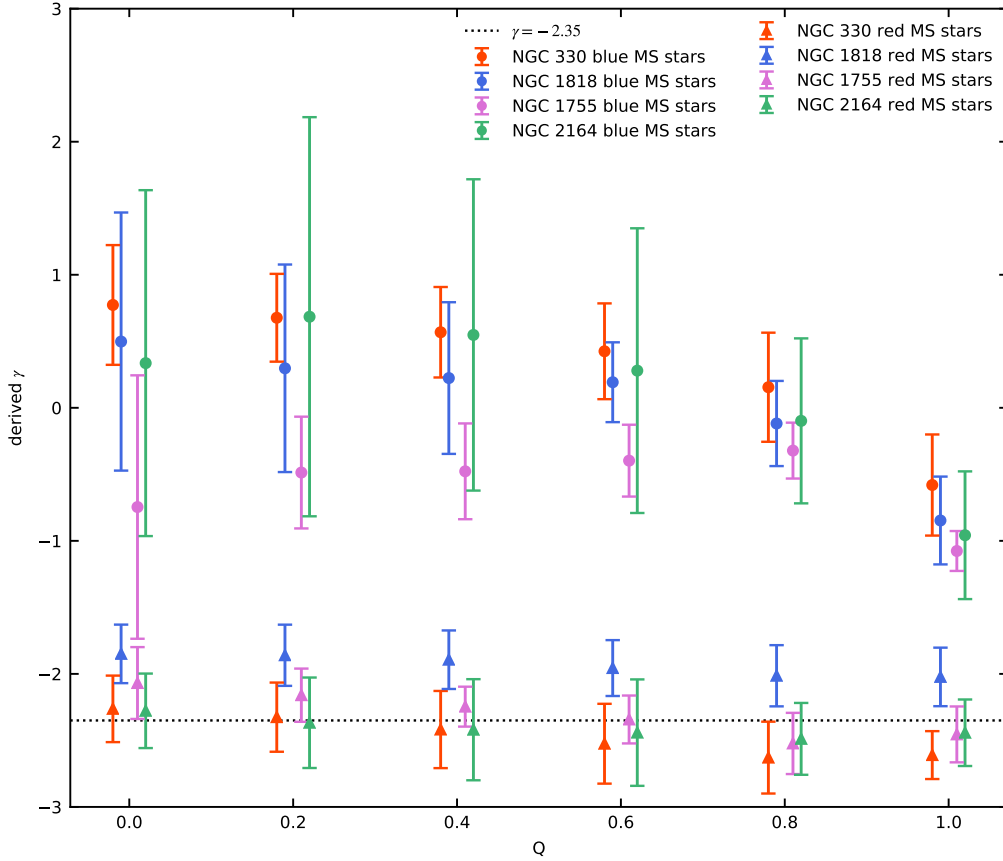
Supplementary Figure 13: Dependence of the mass function slope on the borderline between blue and red main-sequence stars. The borderline is obtained by shifting the isochrone for the blue main sequence by Q times the color separation between the isochrones for the blue and the red main sequences. We consider Q values between 0 and 1, in intervals of 0.2. The filled circles and triangles with error bars denote the derived mass function slope for the blue and the red main-sequence stars with their 1σ errors, respectively. Different colors correspond to different clusters. We avoid to plot the errorbars at the same Q values to make them distinct. The black dashed line marks the slope of the Salpeter IMF $\gamma = -2.35$.
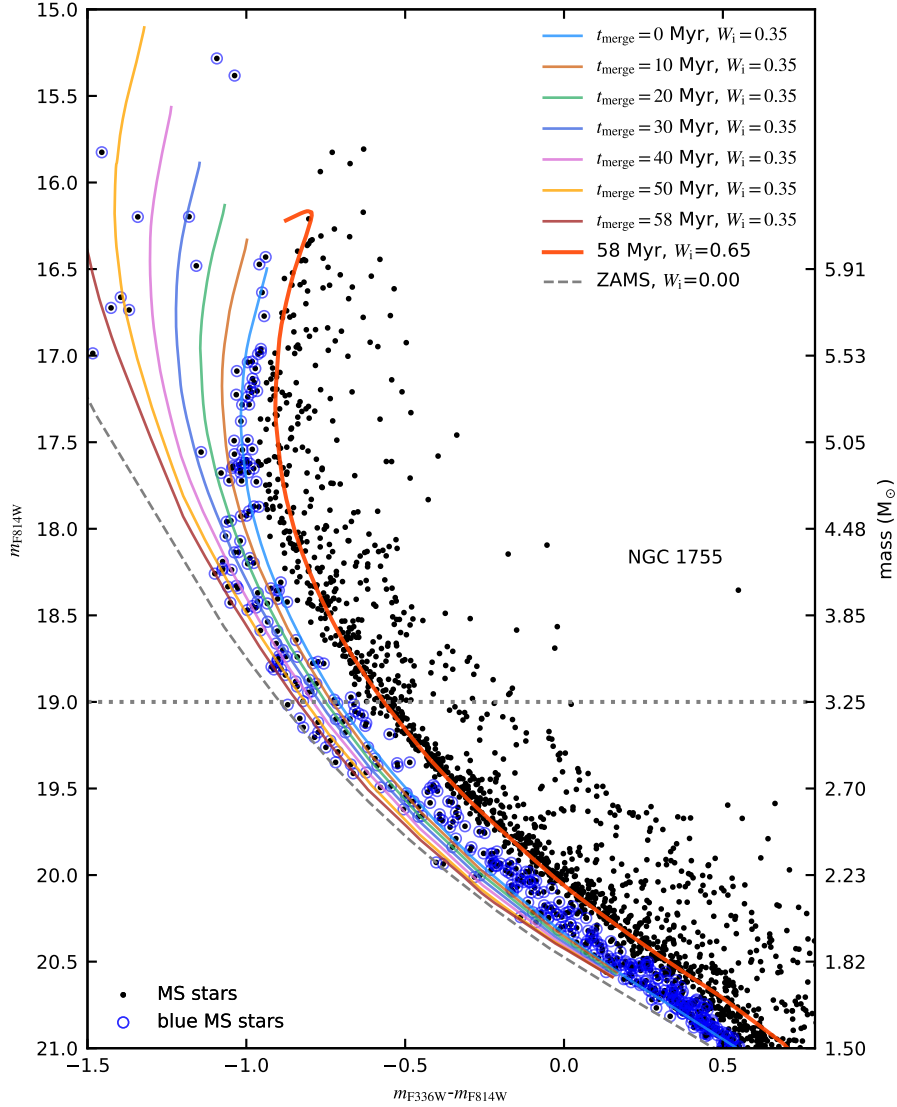
Supplementary Figure 14: Lines of constant merger time in the color-magnitude diagram. The distribution of the main-sequence stars in NGC 1755 is shown, with blue open circles indicating blue main-sequence stars. Solid lines of given colors provide the location of merger products which formed from equal-mass binaries at the indicated time (see color scale) with 35% of critical rotation, and were then evolved to the current cluster age. The blue main-sequence stars above the grey horizontal dotted line are considered in the merger time estimation (see Supplementary Information E). The isochrone fit to the red MS (solid red line), and the resulting zero-age main-sequence line (dashed grey), are as in Fig. 1b.
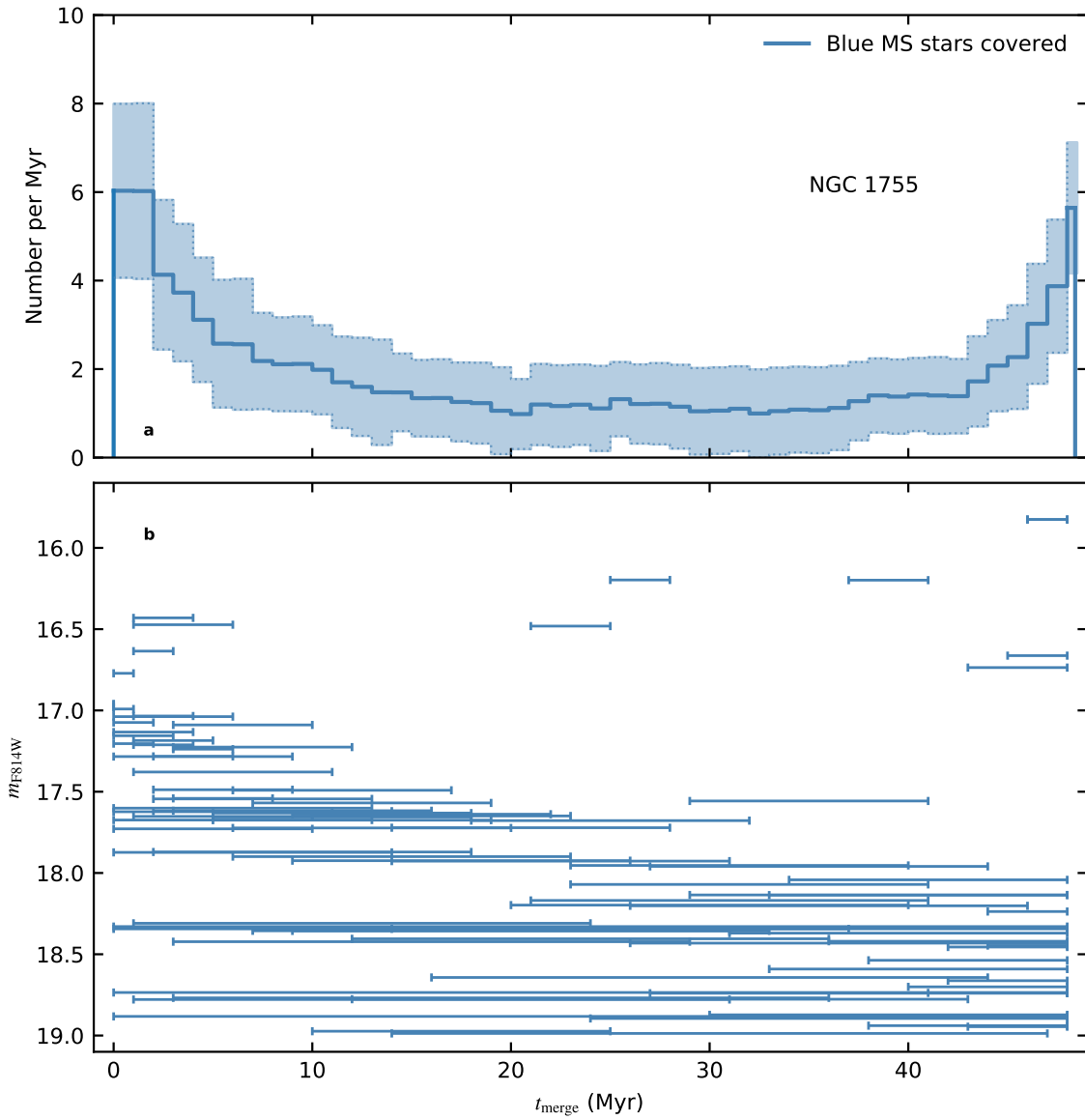
Supplementary Figure 15: Merger history of the blue main-sequence stars in NGC 1755 based on alternative initial rotational velocities (see Supplementary Figure 7a). The plots are the same as Fig. 4.
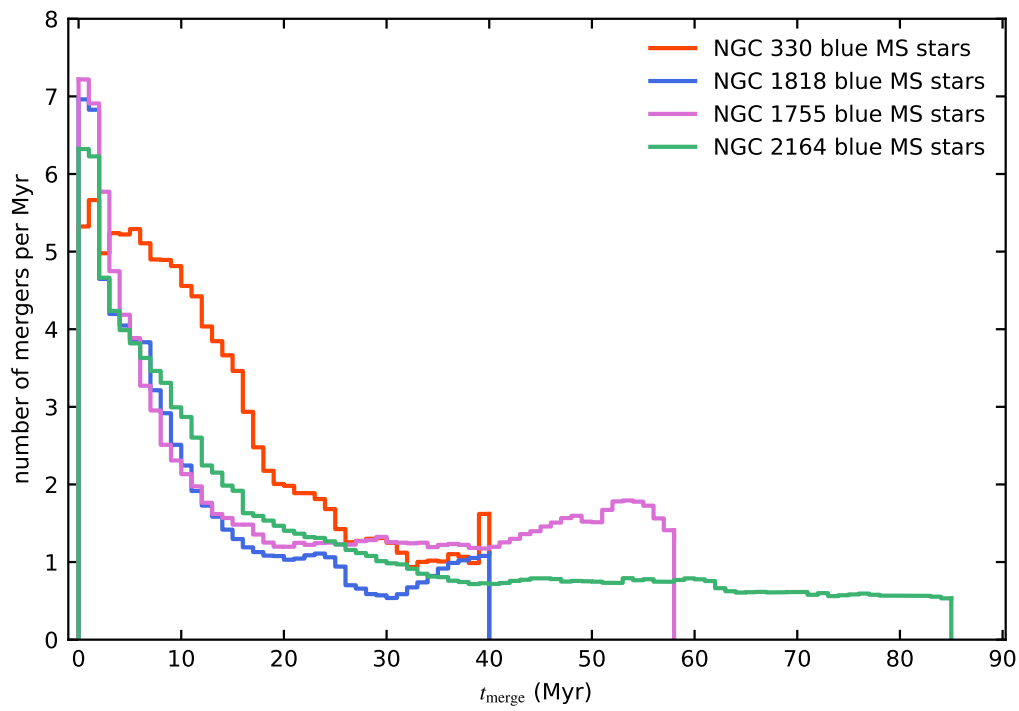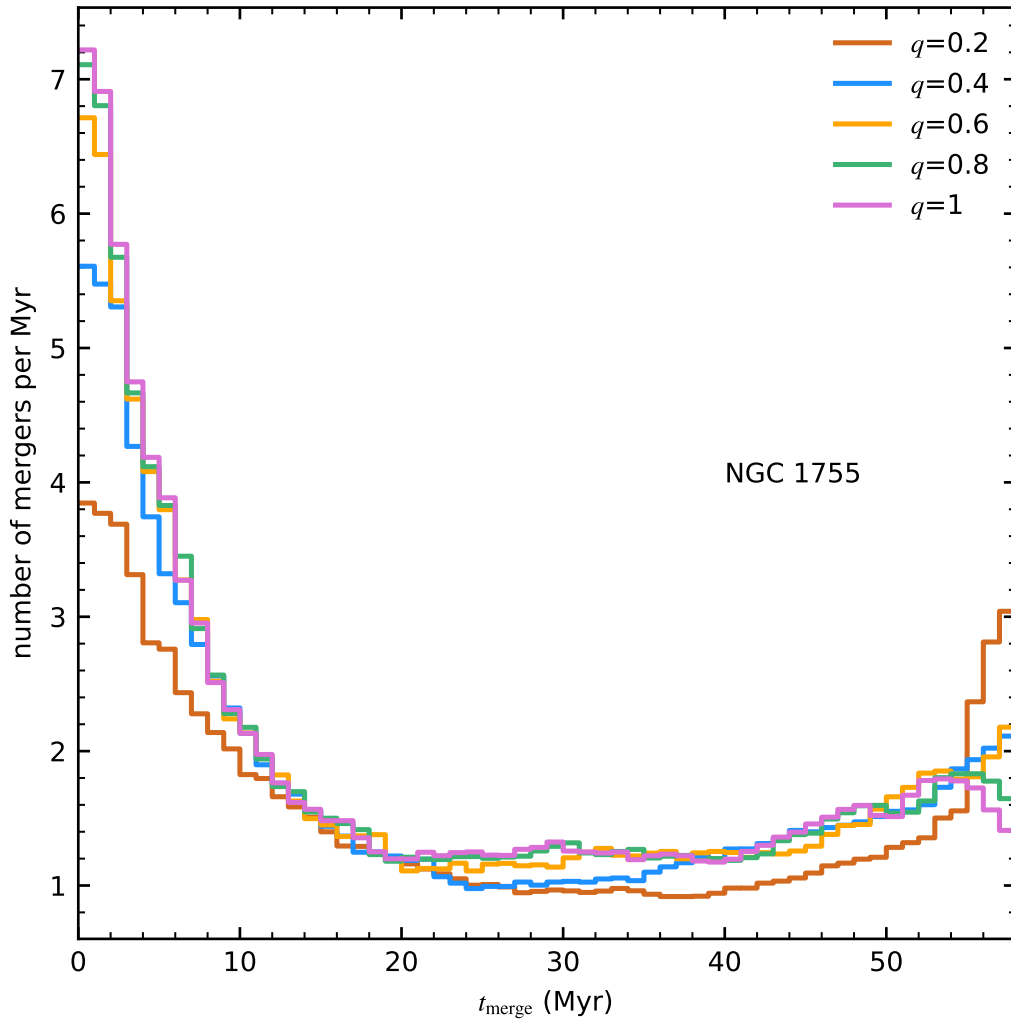
Supplementary Figure 16: Merger history of the blue main-sequence stars in four young Magellanic Cloud clusters. Different colors correspond to different star clusters.
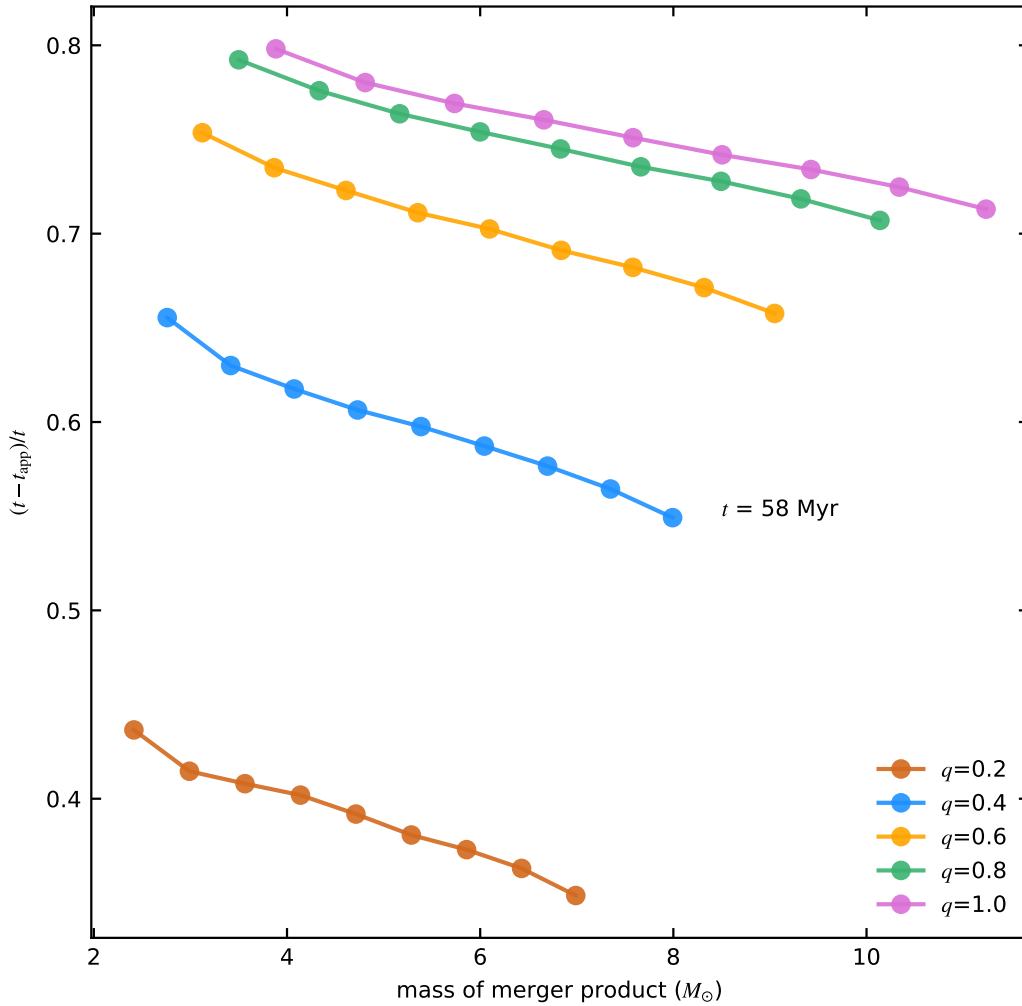
Supplementary Figure 17: Relative rejuvenation for different post-merger stellar masses and pre-merger mass ratios. t is the cluster age of NGC 1755, which also indicates the most recent incidence time of the merger. t_{app} is the apparent age of the merger product as measured by single star isochrones, for a fixed merger time of $t = 58$ Myr. The five lines correspond to five different mass ratios as indicated by their color (see legend). Each dot on the line corresponds to one computed binary model (see Supplementary Information E).
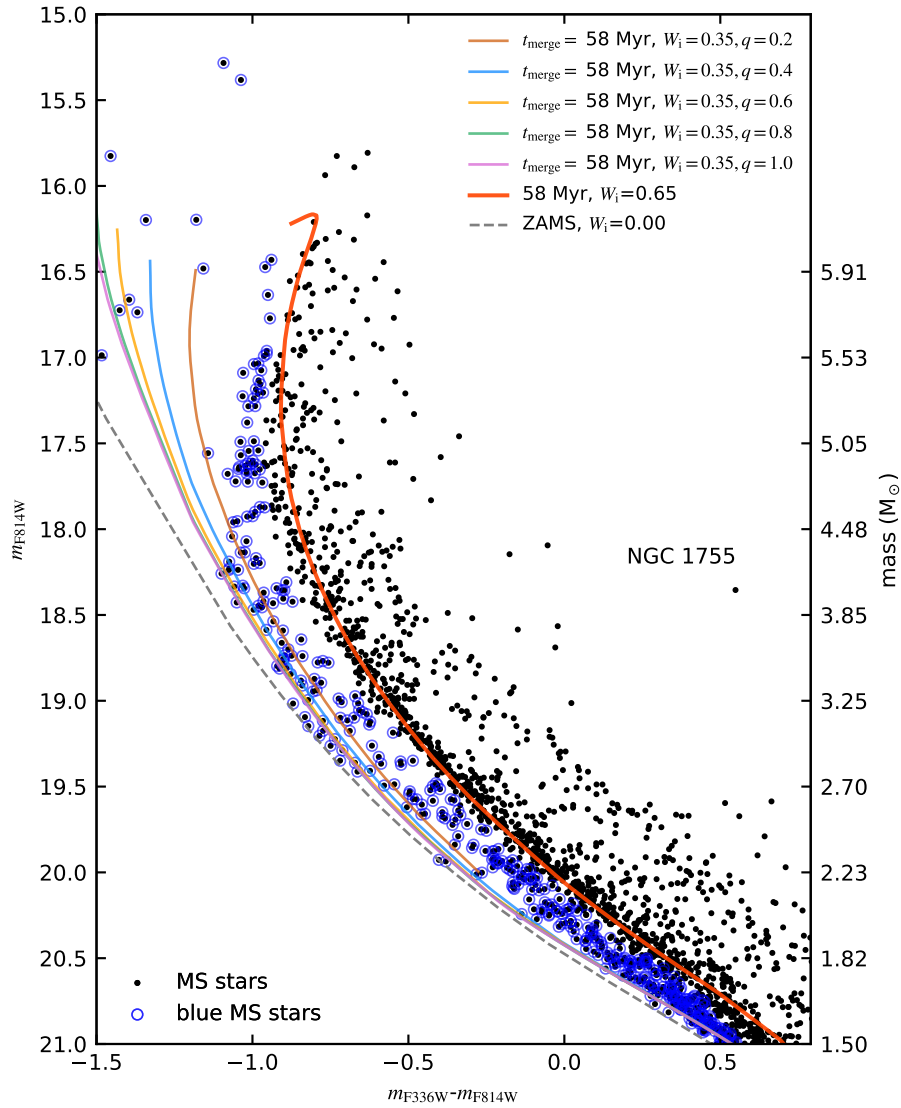
Supplementary Figure 18: Impact of the pre-merger mass ratio on the position of the merger product in the color-magnitude diagram. The thin solid lines correspond to the merger models rotating at 35% of their critical velocities. Different colors correspond to different mass ratios for the precursor binary models. We only show models of mergers for a merger incidence time of 58 Myr. The isochrone for the red main sequence (thick solid red line), and the zero-age main-sequence line (dashed grey) are the same as in Fig. 1b.

Supplementary Figure 19: Effect of the pre-merger mass ratio on the derived merger history. Different colors show the results of the binary merger models with different initial mass ratios.
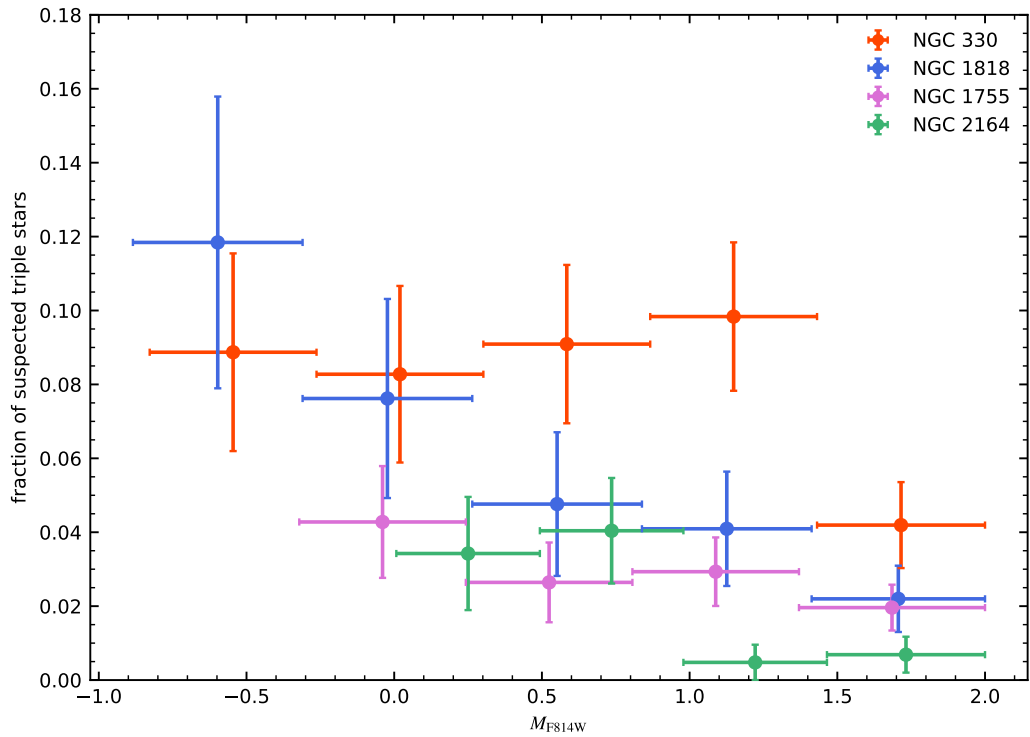
Supplementary Figure 20: Fraction of triple stars (or higher order multiples) in four young Magellanic Cloud clusters. The estimations are based on the equal-mass binary lines in the color-magnitude diagrams (see Fig.1b, and Supplementary Figure 5). We consider absolute magnitude for stars in four young Magellanic Cloud clusters in different magnitude intervals. The horizontal width of the error bars correspond to the magnitude intervals, while the vertical error bars reflect the Poisson error.